INTERNATIONAL JOURNAL FOR NUMERICAL METHODS IN FLUIDS
Int. J. Numer. Meth. Fluids 2007; **54**:609–637
Published online 16 May 2007 in Wiley InterScience (www.interscience.wiley.com). DOI: 10.1002/fld.1476

Computation of turbulent flows using a finite calculus–finite element formulation

E. Oñate*,†, A. Valls and J. García

International Center for Numerical Methods in Engineering (CIMNE), Technical University of Catalonia (UPC), Gran Capitán s/n, 08034 Barcelona, Spain

SUMMARY

We present a formulation for analysis of turbulent incompressible flows using a stabilized finite element method (FEM) based on the finite calculus (FIC) procedure. The stabilization terms introduced by the FIC approach allow to solve a wide range of fluid flow problems at different Reynolds numbers, including turbulent flows, without the need of a turbulence model. Examples of application of the FIC/FEM formulation to the analysis of 2D and 3D incompressible flows at large Reynolds numbers exhibiting turbulence features are presented. Copyright © 2007 John Wiley & Sons, Ltd.

Received 19 January 2007; Revised 8 February 2007; Accepted 8 February 2007

KEY WORDS: turbulent flows; finite calculus; finite element method

1. INTRODUCTION

Stabilized finite element method (FEM) have been successfully used in the past to solve a wide range of fluid mechanics problems [1–28]. The intrinsic dissipative properties of the stabilization terms (which can be interpreted as an additional viscosity) typically suffice to yield good results for low and moderate values of the Reynolds number (Re). For high values of Re most stabilized FEM fail to provide physically sound results and the numerical solution is often unstable or inaccurate. The introduction of a turbulence model is then mandatory in order to obtain meaningful results.

The relationship between the dissipation introduced by a turbulence model and the intrinsic dissipative properties of stabilized FEM is an open topic which is attracting increasing attention in the CFD community [29–34]. It is clear that both remedies (the turbulence model and the

*Correspondence to: E. Oñate, International Center for Numerical Methods in Engineering (CIMNE), Technical University of Catalonia (UPC), Gran Capitán s/n, 08034 Barcelona, Spain.
†E-mail: onate@cimne.upc.edu

Contract/grant sponsor: Publishing Arts Research Council; contract/grant number: 98-1846389
Contract/grant sponsor: Consolider Programme of the Ministerio de Educación y Ciencia of Spain

stabilization terms) play a similar role in the numerical solution, i.e. that of ensuring a solution which is 'physically correct' and as accurate as possible.

This paper extends the work recently presented by Oñate *et al.* [35, 36] where an enhanced stabilized FEM for incompressible flows was derived *via* finite calculus (FIC). The FIC approach is based on expressing the balance laws in mechanics in a domain of finite size. This introduces additional terms in the classical differential equations of momentum and mass balance of infinitesimal fluid mechanics [37–39]. The FIC terms are a function of *characteristic length dimensions* related to the finite element sizes and also to the values of the numerical solution. The FIC terms in the modified governing equations provide the necessary stabilization to the discrete equations obtained *via* the standard Galerkin FEM. The resulting FIC/FEM formulation allows to use low-order finite elements (such as linear triangles and tetrahedra) with an equal order approximation for the velocity and the pressure variables [35–39].

This paper shows that the nonlinear stabilization terms introduced by the FIC formulation into the momentum equations have a form of a nonlinear viscosity which is a function of the velocity and the velocity gradients. On the other hand, the FIC formulation introduces a Laplacian of pressure term into the mass balance equation. The resulting FIC/FEM formulation can be used to solve accurately high *Re* number flows *without the need of introducing any turbulence model*. The good results obtained in the examples presented indicate that the (nonlinear) FIC stabilization terms play the role of a turbulent model. The remarkable aspect of this approach is that the FIC equations are derived from basic principles in mechanics, such as balance of momentum and mass over a domain of finite size and, in conjunction with a numerical procedure such as the FEM, they provide a very simple procedure for the analysis of complex fluid mechanics problems.

The outline of the paper is the following. In the next section, the basic concepts of the FIC method are outlined for the simple one-dimensional (1D) advection–diffusion problem. Then, the FIC governing equations for an incompressible viscous flow are derived. A discussion of the stabilization terms introduced by the FIC procedure into the momentum and mass balance equations is presented. The discretization of the FIC governing equations using equal order linear finite elements is described and the matrix form of the element matrices and vectors for 3D fluid flow analysis is detailed. The time integration of the discretized equations using a fractional step scheme is described. The procedure for computing the stabilization parameters is presented. The accuracy of the FIC/FEM formulation for analysis of turbulent flows is verified in two examples of application.

2. FINITE CALCULUS: BASIC CONCEPTS

The FIC method developed by Oñate and co-workers [35–57] is a consistent procedure for reformulating the governing equation in mechanics introducing new terms involving characteristic space and time dimensions into the equations. The modified equations are derived by invoking the balance laws in mechanics in a space–time domain of finite size. The new terms introduced by the FIC approach are essential to obtain physical (stable) numerical solutions for all ranges of the parameters governing the physical problem.

The merit of the modified equations *via* the FIC approach is that they lead to stabilized schemes *using any numerical method*. Moreover, many stabilized numerical methods typically used in practice can be *recovered* using the FIC equations [37, 43].

DOI: 10.1002/fld

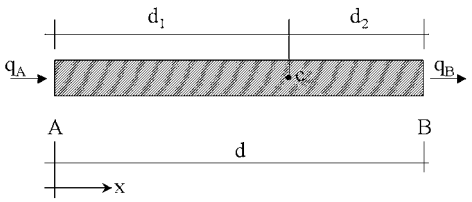

Figure 1. Equilibrium of fluxes in a space balance domain of finite size.

The FIC/FEM formulation has proven to be very effective for the solution of a wide class of problems, such as convection–diffusion [37–45] and convection–diffusion–reaction problems [46–48] involving arbitrary high gradients, incompressible flow problems accounting for free surface effects and fluid–structure interaction situations [49–54] and quasi and fully incompressible problems in solid mechanics [55–57].

In order to introduce the basic concepts of the FIC method, we will consider a steady-state convection–diffusion problem in a 1D domain Ω of length L. The equation of balance of fluxes in a subdomain of size d belonging to Ω (Figure 1) is

$$q_A - q_B = 0 \tag{1}$$

where q_A and q_B are the incoming and outgoing fluxes at points A and B, respectively. The flux q includes both convective and diffusive terms; i.e. $q = u\phi - k\mathrm{d}\phi/\mathrm{d}x$, where ϕ is the transported variable (i.e. the temperature in a thermal problem), u is the velocity and k is the diffusivity of the material. For simplicity, the density and the specific heat constant have been assumed to have a unit value.

Let us express now the fluxes q_A and q_B in terms of the flux at an arbitrary point C within the balance domain (Figure 1). Expanding q_A and q_B in Taylor series around point C up to second-order terms gives

$$q_A = q_C - d_1 \frac{\mathrm{d}q}{\mathrm{d}x}\bigg|_C + \frac{d_1^2}{2}\frac{\mathrm{d}^2 q}{\mathrm{d}x^2}\bigg|_C + O(d_1^3), \quad q_B = q_C + d_2 \frac{\mathrm{d}q}{\mathrm{d}x}\bigg|_C + \frac{d_2^2}{2}\frac{\mathrm{d}^2 q}{\mathrm{d}x^2}\bigg|_C + O(d_2^3) \tag{2}$$

Substituting Equation (2) into Equation (1) gives after simplification

$$\frac{\mathrm{d}q}{\mathrm{d}x} - \underline{\frac{h}{2}\frac{\mathrm{d}^2 q}{\mathrm{d}x^2}} = 0 \tag{3}$$

where $h = d_1 - d_2$ and all the derivatives are computed at the arbitrary point C.

Standard calculus theory assumes that the domain d is of infinitesimal size and the resulting balance equation is simply $\mathrm{d}q/\mathrm{d}x = 0$. We will relax this assumption and allow the space balance domain to have a *finite size*. The new balance equation (3) incorporates now the underlined term which introduces the *characteristic length* h.

Distance h in Equation (3) is as a free parameter depending on the location of point C within the balance domain. Note that $-d \leqslant h \leqslant d$ and, hence, h can take a negative value. At the discrete solution level the domain d should be replaced by the balance domain around a node. This gives for an equal size discretization $-l^{\mathrm{e}} \leqslant h \leqslant l^{\mathrm{e}}$ where l^{e} is the element or cell dimension. Equation (3)

DOI: 10.1002/fld

is the *exact balance equation* (up to second-order terms) for any 1D domain of finite size. The FIC balance equations can be used to derive numerical schemes with enhanced properties simply by computing the characteristic length parameter from an adequate 'optimality' rule, such as requiring an smaller error in the numerical solution [40–48].

Consider, for instance, the 1D convection–diffusion problem. Neglecting third-order derivatives of ϕ, Equation (3) can be rewritten in terms of ϕ as

$$-u\frac{\mathrm{d}\phi}{\mathrm{d}x}+\left(k+\frac{uh}{2}\right)\frac{\mathrm{d}^2\phi}{\mathrm{d}x^2}=0 \tag{4}$$

We see clearly that the FIC method introduces *naturally* an additional diffusion term in the standard convection–diffusion equation. This is the basis of the popular 'artificial diffusion' procedure [1, 2, 10, 25] where the characteristic length h is typically expressed as a function of the cell or element dimension. The *critical* value of h can be computed by requiring that the numerical solution of Equation (4) is physically meaningful [1, 2, 10, 25, 37–43].

Equation (3) can be extended to account for source terms. The resulting FIC balance equation can then be written in compact form as [37]

$$r-\underline{\frac{h}{2}\frac{\mathrm{d}r}{\mathrm{d}x}}=0 \tag{5}$$

with

$$r:=-u\frac{\mathrm{d}\phi}{\mathrm{d}x}+\frac{\mathrm{d}}{\mathrm{d}x}\left(k\frac{\mathrm{d}\phi}{\mathrm{d}x}\right)+Q \tag{6}$$

where Q is the external source. Note that for $h=0$ the standard heat balance equation of the infinitesimal theory ($r=0$) is recovered.

The essential (Dirichlet) boundary condition for Equation (5) is $\phi=\bar{\phi}$ on Γ_ϕ where Γ_ϕ is the boundary where the prescribed value $\bar{\phi}$ is imposed. For consistency, a stabilized Neumann boundary condition must be obtained as described next.

Let us consider a balance domain next to a Neumann boundary point B (Figure 2).

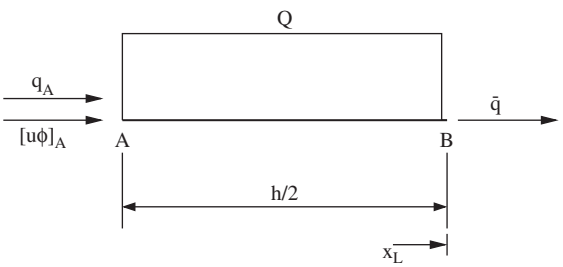

Figure 2. Balance domain next to a Neumann boundary point B.

DOI: 10.1002/fld

The length of the balance segment AB next to a Neumann boundary is taken as one half of the characteristic length h for the interior domain. The balance equation, assuming a constant distribution for the source Q, is

$$\bar{q} - q(x_A) - [u\phi]_A - \frac{h}{2}Q = 0 \tag{7}$$

where $\bar{q}$ is the prescribed total flux at $x = L$ and $x_A = x_B - h/2$.

Using a second-order expansion for the advective and diffusive fluxes at point A gives [37]

$$-u\phi + k\frac{\mathrm{d}\phi}{\mathrm{d}x} + \bar{q} - \underline{\frac{h}{2}r} \quad \text{on } x = L \tag{8}$$

where r is given by Equation (6). Again for $h = 0$, the infinitesimal form of the 1D Neumann boundary condition is obtained.

It is important to recall that the underlined terms in Equations (5) and (8) introduce the necessary stabilization in the discrete solution *using whatever numerical scheme* [37, 39].

Quite generally the FIC equations can be written for any problem in mechanics as

$$r_i - \frac{h_{ij}}{2}\frac{\partial r_i}{\partial x_j} - \frac{\delta}{2}\frac{\partial r_i}{\partial t} = 0, \quad i = 1, n_\mathrm{b}, \quad j = 1, n_\mathrm{d} \tag{9}$$

where r_i is the ith standard differential equation of the infinitesimal theory, h_{ij} are characteristic length parameters, δ is a characteristic time parameter and n_b and n_d are, respectively, the number of balance equations and the number of space dimensions of the problem (i.e. $n_\mathrm{d} = 3$ for 3D problems). The usual sum convention for repeated indexes is used in the text unless otherwise specified. In this work, the term involving the time parameter δ will be neglected in the FIC equations.

3. FIC EQUATIONS FOR AN INCOMPRESSIBLE VISCOUS FLOW

The FIC momentum equations are obtained by expressing the balance of momentum along each of the space directions in a domain of 'finite' size. Figure 3 shows a typical finite domain for a two-dimensional (2D) problem. Following a procedure analogous to that explained in the previous

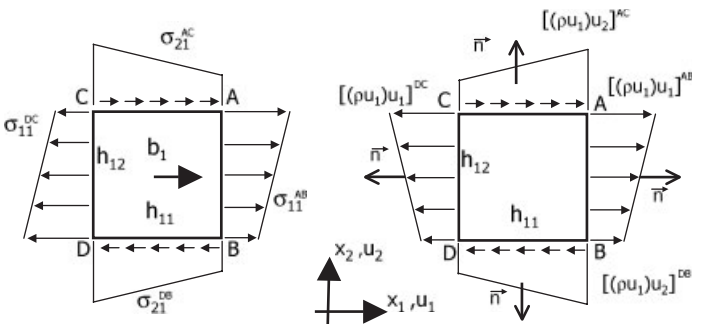

Figure 3. Finite domain where balance of momentum is imposed along the horizontal direction.

DOI: 10.1002/fld

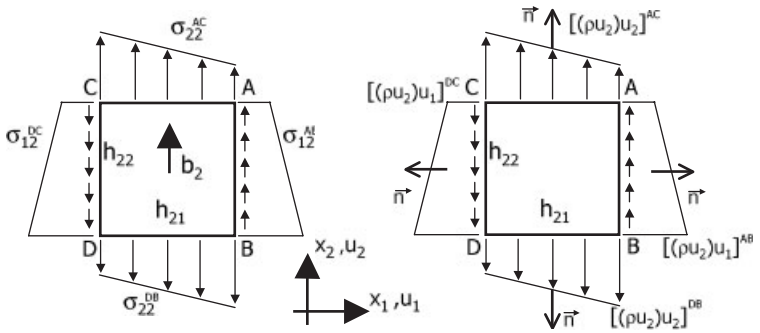

Figure 4. Finite domain where balance of momentum is imposed along the vertical direction.

section for the 1D advection–diffusion problem the balance equation along the ith space direction can be written as

$$\sum f_i \, \mathrm{d}\Omega = \frac{\partial}{\partial t} \int_\Omega \rho u_i \, \mathrm{d}\Omega + \int_\Gamma (\rho u_i) \mathbf{u}^{\mathrm{T}} \mathbf{n} \, \mathrm{d}\Gamma, \quad i = 1, n_{\mathrm{d}} \tag{10}$$

where ρ is the density, which is assumed to be constant hereafter, u_i is the component of the velocity along the ith space direction, $\mathbf{u} = [u_1, u_2, u_3]^{\mathrm{T}}$ is the velocity vector, $\mathbf{n}$ is the unit vector normal to the domain boundary and f_i includes the forces due to the stresses acting on the boundary of the balance domain and the body forces per unit area b_i (Figures 3 and 4).

Expressing the values of the momentum and force terms at the corner points of the balance domain in terms of the values at the corner point A using higher-order Taylor expansions in the space directions and retaining second-order terms, gives after some algebra the FIC momentum equations along the ith coordinate direction as [37]

$$\bar{r}_{m_i} - \underline{\frac{1}{2} h_{ij} \frac{\partial \bar{r}_{m_i}}{\partial x_j}} = 0, \quad i, j = 1, n_{\mathrm{d}} \tag{11}$$

where

$$\bar{r}_{m_i} := \rho \left[\frac{\partial u_i}{\partial t} + \frac{\partial}{\partial x_j} (u_i u_j) \right] - \frac{\partial \sigma_{ij}}{\partial x_j} - b_i \tag{12}$$

with $\sigma_{ij} = s_{ij} - p\delta_{ij}$, where p is the pressure, δ_{ij} is the Dirac delta and s_{ij} are the viscous stresses related to the velocities by the standard expression

$$s_{ij} = 2\mu \left(\varepsilon_{ij} - \delta_{ij} \frac{1}{3} \frac{\partial u_k}{\partial x_k} \right) \tag{13}$$

where

$$\varepsilon_{ij} = \frac{1}{2} \left(\frac{\partial u_i}{\partial x_j} + \frac{\partial u_j}{\partial x_i} \right) \tag{14}$$

DOI: 10.1002/fld

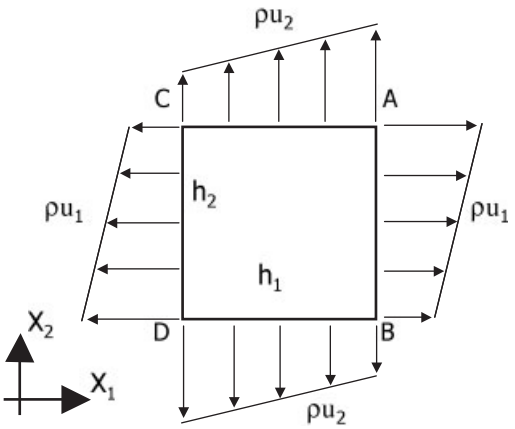

Figure 5. Finite domain where balance of mass is enforced.

Note that distance h_{12} is arbitrary when writing the balance of momentum along the x_1 direction. The same applies for the distance h_{21} when deriving the balance equation along the x_2 direction. Thus, in general, $h_{12} \neq h_{21}$.

The convective term in the expression of $\bar{r}_{m_i}$ of Equation (12) is written in conservation form, as deduced from the FIC momentum balance equations. A simplified form of $\bar{r}_{m_i}$ can be written by introducing the incompressibility condition ($\partial u_i / \partial x_i = 0$) into the convective term of $\bar{r}_{m_i}$ and using the split of the stresses σ_{ij} into their deviatoric and pressure components giving

$$r_{m_i} - \underline{\frac{1}{2} h_{ij} \frac{\partial r_{m_i}}{\partial x_j}} = 0, \quad i, j = 1, n_{\mathrm{d}} \tag{15}$$

with

$$r_{m_i} := \rho \left(\frac{\partial u_i}{\partial t} + u_j \frac{\partial u_i}{\partial x_j} \right) + \frac{\partial p}{\partial x_i} - \frac{\partial s_{ij}}{\partial x_j} - b_i \tag{16}$$

The two forms of the FIC balance equations (11) and (15) are identical for the exact incompressible solution. Both forms will be used to the advantage of each derivation step in the following sections.

3.1. Mass balance equation

The FIC mass balance equation is obtained by invoking the balance of mass in the finite domain of Figure 5

$$\int_{\Gamma} \rho \mathbf{u}^{\mathrm{T}} \mathbf{n} \, \mathrm{d}\Gamma = 0 \tag{17}$$

DOI: 10.1002/fld

Expanding the values of ρu_i at the corner points in terms of the value at the corner point A gives the FIC mass balance equation as [37, 38]

$$\varepsilon_v - \underline{\frac{1}{2} h_j \frac{\partial \varepsilon_v}{\partial x_j}} = 0, \quad j = 1, n_{\mathrm{d}} \tag{18a}$$

with

$$\varepsilon_v = \frac{\partial u_i}{\partial x_i} \tag{18b}$$

Note that a matrix form of the characteristic distances is not obtained in this case as the mass balance equation expresses the conservation of the mass in the domain *ABCD* of Figure 5 with dimensions h_1 and h_2. Distances h_1 and h_2 are in general different from the distances h_{ij} defining the domain where balance of momentum is enforced. In the following, we will assume that $h_1 = h_{11}$ and $h_2 = h_{22}$ for simplicity.

3.2. Boundary conditions

The FIC Neumann boundary conditions are obtained by expressing the balance of momentum in a domain of finite size adjacent to a boundary Γ_t where the surface tractions t_i act. After some algebra we obtain [37, 38]

$$n_j \sigma_{ij} - t_i + \underline{\tfrac{1}{2} h_{ij} n_j r_{m_i}} = 0 \quad \text{on } \Gamma_t, \quad j = 1, n_{\mathrm{d}} \text{ no sum in } i \tag{19a}$$

In Equation (19a) the h_{ij} distances define the domain where equilibrium of boundary tractions is established. The boundary condition on the Dirichlet boundary Γ_u is the standard one

$$u_j - u_j^p = 0 \quad \text{on } \Gamma_u \tag{19b}$$

Note that in the discretized problem the characteristic distances become the order of the typical element dimensions. The infinitesimal form of the fluid mechanics equations is recovered by making these distances equal to zero.

Equations (11)–(19) are the starting points for deriving stabilized FEM for solving the incompressible Navier–Stokes equations. The underlined FIC terms in Equations (11) (or (15)) and (19a) are essential to overcome the numerical instabilities due to the convective terms in the momentum equations, whereas the underlined terms in Equation (18a) take care of the instabilities due to the incompressibility constraint. An important feature of the FIC formulation is that it allows to use equal order interpolation for the velocity and pressure variables [38, 54].

4. A DISCUSSION OF THE STABILIZATION TERMS IN THE FIC EQUATIONS

The compact residual forms of the FIC equations of momentum balance (Equations (11) or (15)) and mass balance (Equation (18a)) hide the relevant terms that contribute to the stabilization of the numerical solution for all flow regimes. We will show next that the FIC terms introduce a *nonlinear anisotropic viscosity* into the standard momentum equations of the infinitesimal theory. Also, it is shown that the FIC terms in the mass balance equation introduce a *pressure Laplacian* term.

DOI: 10.1002/fld

4.1. Momentum equations

Let us write the ith FIC momentum equation of Equation (15) as

$$\rho\left[\frac{\partial u_i}{\partial t}+u_j\frac{\partial u_i}{\partial x_j}\right]+\frac{\partial p}{\partial x_i}-\frac{\partial s_{ij}}{\partial x_j}-b_i-\frac{h_{ik}}{2}\frac{\partial}{\partial x_k}\left[c_i+\rho u_j\frac{\partial u_i}{\partial x_j}\right]=0 \tag{20}$$

where

$$c_i:=\rho\frac{\partial u_i}{\partial t}-\frac{\partial \sigma_{ij}}{\partial x_j}-b_i \tag{21}$$

is termed the *convective projection* term. Note that in the infinitesimal limit

$$r_{m_i}:=c_i+\rho u_j\frac{\partial u_i}{\partial x_j}=0 \tag{22}$$

Substituting the expression of the viscous stresses of Equation (13) into Equation (20) and using Equation (14) yields after small algebra

$$\rho\left[\frac{\partial u_i}{\partial t}+u_j\frac{\partial u_i}{\partial x_j}\right]+\frac{\partial p}{\partial x_i}-\frac{\partial}{\partial x_k}[\mu\delta_{kj}+\bar{\mu}_{kj}]\frac{\partial u_i}{\partial x_j}-b_i-\frac{h_{ik}}{2}\frac{\partial c_i}{\partial x_k}+\mu\frac{\partial \varepsilon_v}{\partial x_i}=0 \tag{23}$$

where

$$\bar{\mu}_{kj}=\frac{\rho u_j h_{ik}}{2} \tag{24}$$

In the derivation of Equation (23) we have assumed that the space derivatives of the characteristic lengths h_{ij} are zero.

Equation (23) shows clearly that the FIC formulation introduces the following new terms into the ith momentum equation of the infinitesimal theory:

(a) an additional (nonlinear) anisotropic viscosity $\bar{\mu}_{kj}$ given by Equation (24) and
(b) a convective projection term of value $-h_{ik}/2(\partial c_i/\partial x_k)$.

The last term in Equation (23) involving ε_v is usually disregarded in practice. We have found, however, that retaining this term is very important in free surface viscous flows [58]. For this reason, the full compact (residual) form of Equations (11) or (15) is used in practice.

4.2. Mass balance equation

The FIC momentum balance equation (11) is written as (assuming the viscosity μ to be constant)

$$\rho\left[\frac{\partial u_i}{\partial t}+u_j\frac{\partial u_i}{\partial x_j}\right]+\rho u_i\varepsilon_v+\frac{\partial p}{\partial x_i}-\frac{\partial}{\partial x_j}(2\mu\varepsilon_{ij})+\frac{2}{3}\mu\frac{\partial \varepsilon_v}{\partial x_i}-b_i-\frac{h_{ij}}{2}\frac{\partial \bar{r}_{m_i}}{\partial x_j}=0 \tag{25}$$

From the FIC mass balance equation (18a) we deduce

$$\varepsilon_v=\frac{h_j}{2}\frac{\partial \varepsilon_v}{\partial x_j} \tag{26}$$

DOI: 10.1002/fld

Substituting ε_v from Equation (26) into (25) gives after small algebra

$$\frac{\partial \varepsilon_v}{\partial x_i} = \frac{1}{a_i}\left[\frac{h_{ij}}{2}\frac{\partial \bar{r}_{m_i}}{\partial x_j} - r_{m_i} - \rho\frac{u_i h_k}{2}\frac{\partial \varepsilon_v}{\partial x_k}\right], \quad i \neq k \tag{27}$$

with

$$a_i = \frac{2\mu}{3} + \rho\frac{u_i h_i}{2} \quad \text{no sum in } i \tag{28}$$

We note that all terms in Equation (27) vanish for the exact solution. On this basis, the following simplified expression is chosen for $\partial\varepsilon_v/\partial x_i$:

$$\frac{\partial \varepsilon_v}{\partial x_i} = \frac{h_{ii}}{2a_i}\frac{\partial r_{m_i}}{\partial x_i} \quad \text{no sum in } i \tag{29}$$

Substituting Equation (29) into (18a) gives the following useful expression for the FIC mass balance equation incorporating the momentum equations r_{m_i}:

$$\varepsilon_v - \sum_{i=1}^{n_d} \tau_i \frac{\partial r_{m_i}}{\partial x_i} = 0 \tag{30}$$

with

$$\tau_i = \left(\frac{8\mu}{3h_{ii}^2} + \frac{2\rho u_i}{h_{ii}}\right)^{-1} \tag{31}$$

Note that in Equation (31) the assumption $h_i = h_{ii}$ has been used.

The τ_i's in Equation (33) when multiplied by the density are equivalent to the *intrinsic time parameters*, seen extensively in the stabilization literature [1–28]. The interest of Equation (30) is that it introduces a Laplacian of pressure term into the mass balance equations through the first derivative of r_{m_i}. To show this clearly it is convenient to express the r_{m_i} terms as

$$r_{m_i} = \frac{\partial p}{\partial x_i} + \pi_i \tag{32}$$

where π_i are termed the *pressure gradient projections*. The exact expression of π_i is deduced by substracting the pressure gradient terms from the standard momentum equations, i.e.

$$\pi_i := \rho\left[\frac{\partial u_i}{\partial t} + u_j\frac{\partial u_i}{\partial x_j}\right] - \frac{\partial}{\partial x_j}(2\mu s_{ij}) - b_i \tag{33}$$

This form of π_i will not be, however, used in practice as the nodal values of π_i are directly computed from the projection of the pressure gradients, as explained in the next section.

DOI: 10.1002/fld

Substituting the expression of r_{m_i} of Equation (32) into Equation (30) gives

$$\varepsilon_v - \sum_{i=1}^{n_d} \tau_i \frac{\partial}{\partial x_i}\left(\frac{\partial p}{\partial x_i} + \pi_i\right) = \varepsilon_v - \sum_{i=1}^{n_d} \tau_i \left[\frac{\partial^2 p}{\partial x_i^2} + \frac{\partial \pi_i}{\partial x_i}\right] = 0 \tag{34}$$

Equation (33) shows that the FIC formulation introduces naturally a Laplacian of pressure term into the mass balance equation. The consistency of the approach is ensured by the pressure gradient projection terms π_i, as the bracketed terms in Equation (34) are equal to the momentum equations and, therefore, they vanish as these equations are satisfied for the 'exact' solution.

5. INTEGRAL FORM OF THE FIC GOVERNING EQUATIONS

The weighted residual form of the momentum and mass balance equations (Equations (15) and (30)) is

$$\int_\Omega \delta u_i \left[r_{m_i} - \frac{h_{ij}}{2}\frac{\partial r_{m_i}}{\partial x_j}\right] d\Omega + \int_{\Gamma_t} \delta u_i \left(\sigma_{ij} n_j - t_i + \frac{h_{ij}}{2} n_j r_{m_i}\right) d\Gamma = 0 \tag{35a}$$

$$\int_\Omega q \left[\varepsilon_v - \sum_{i=1}^{n_d} \tau_i \frac{\partial r_{m_i}}{\partial x_i}\right] d\Omega = 0 \tag{35b}$$

where δu_i and q are arbitrary weighting functions representing virtual velocities and virtual pressure fields. Integrating by parts the terms involving the derivatives of r_{m_i} in Equations (34) gives

$$\int_\Omega \delta u_i r_{m_i}\, d\Omega + \int_{\Gamma_t} \delta u_i (\sigma_{ij} n_j - t_i)\, d\Gamma + \int_\Omega \frac{h_{ij}}{2}\frac{\partial \delta u_i}{\partial x_j} r_{m_i}\, d\Omega = 0 \tag{36a}$$

$$\int_\Omega q \varepsilon_v\, d\Omega + \int_\Omega \left[\sum_{i=1}^{n_d} \tau_i \frac{\partial q}{\partial x_i} r_{m_i}\right] d\Omega - \int_\Gamma \left[\sum_{i=1}^{n_d} q \tau_i n_i r_{m_i}\right] d\Gamma = 0 \tag{36b}$$

We will neglect hereonwards the third integral in Equation (36b) by assuming that r_{m_i} is negligible on the boundaries. The deviatoric stresses and the pressure terms in the first integral of Equation (36a) are integrated by parts in the usual manner. The resulting momentum and mass balance equations are

$$\int_\Omega \left[\delta u_i \rho \left(\frac{\partial u_i}{\partial t} + u_j \frac{\partial u_i}{\partial x_j}\right) + \frac{\partial \delta u_i}{\partial x_j}\left(s_{ij} - \delta_{ij} p\right)\right] d\Omega - \int_\Omega \delta u_i b_i d\Omega$$
$$- \int_{\Gamma_t} \delta u_i t_i\, d\Gamma + \int_\Omega \frac{h_{ij}}{2}\frac{\partial \delta u_i}{\partial x_j} r_{m_i}\, d\Omega = 0 \tag{37a}$$

$$\int_\Omega q \frac{\partial u_i}{\partial x_i}\, d\Omega + \int_\Omega \left[\sum_{i=1}^{n_d} \tau_i \frac{\partial q}{\partial x_i} r_{m_i}\right] d\Omega = 0 \tag{37b}$$

DOI: 10.1002/fld

The computation of the residual terms is simplified if we introduce the convective projections c_i (Equation (22)) and the pressure gradient projections π_i (Equation (32)). We therefore express r_{m_i} in Equations (37a) and (37b) in terms of c_i and π_i, respectively, which then become additional variables. The system of integral equations is now augmented in the necessary number of equations by imposing that the residual r_{m_i} vanishes (in a weighted residual sense) for both forms given by Equations (22) and (32). This gives the final system of governing equation as

$$\int_\Omega \left[\delta u_i \rho \left(\frac{\partial u_i}{\partial t} + u_j \frac{\partial u_i}{\partial x_j}\right) + \frac{\partial \delta u_i}{\partial x_j}(s_{ij} - \delta_{ij} p)\right] \mathrm{d}\Omega - \int_\Omega \delta u_i b_i \, \mathrm{d}\Omega$$
$$- \int_{\Gamma_t} \delta u_i t_i \, \mathrm{d}\Gamma + \int_\Omega \frac{h_{ik}}{2} \frac{\partial(\delta u_i)}{\partial x_k} \left(\rho u_j \frac{\partial u_i}{\partial x_j} + c_i\right) \mathrm{d}\Omega = 0 \tag{38}$$

$$\int_\Omega q \frac{\partial u_i}{\partial x_i} \, \mathrm{d}\Omega + \int_\Omega \sum_{i=1}^{n_\mathrm{d}} \tau_i \frac{\partial q}{\partial x_i} \left(\frac{\partial p}{\partial x_i} + \pi_i\right) \mathrm{d}\Omega = 0 \tag{39}$$

$$\int_\Omega \delta c_i \rho \left(\rho u_j \frac{\partial u_i}{\partial x_j} + c_i\right) \mathrm{d}\Omega = 0 \quad \text{no sum in } i \tag{40}$$

$$\int_\Omega \delta \pi_i \tau_i \left(\frac{\partial p}{\partial x_i} + \pi_i\right) \mathrm{d}\Omega = 0 \quad \text{no sum in } i \tag{41}$$

with $i, j, k = 1, n_\mathrm{d}$. In Equations (40) and (41) δc_i and $\delta \pi_i$ are appropriate weighting functions and the ρ and τ_i weights are introduced for convenience.

Accounting for the convective and pressure gradient projections enforces the consistency of the formulation as it ensures that the stabilization terms in Equations (38) and (39) have a residual form which vanishes for the 'exact' solution. Neglecting these terms can reduce the accuracy of the numerical solution and it makes the formulation more sensitive to the value of the stabilization parameters [54–56].

6. FINITE ELEMENT DISCRETIZATION

We choose C° continuous linear interpolations for the velocities, the pressure, the convective projections c_i and the pressure gradient projections π_i over 3-noded triangles (2D) and 4-noded tetrahedra (3D). The linear interpolations are written as

$$\begin{aligned} u_i &= N^k \bar{u}_i^k, \quad p = N^k \bar{p}^k \\ c_i &= N^k \bar{c}_i^k, \quad \pi_i = N^k \bar{\pi}_i^k \end{aligned} \tag{42}$$

where the sum goes over the number of nodes of each element $n = 3, 4$ for triangles/tetrahedra, $\bar{(\cdot)}^k$ denotes the nodal variables and N^k are the linear shape functions [25, 26].

DOI: 10.1002/fld

Substituting approximations (42) into Equations (38)–(41) and choosing the Galerkin form with $\delta u_i = q = \delta c_i = \delta \pi_i = N^i$ lead to the following system of discretized equations:

$$\mathbf{M}\dot{\bar{\mathbf{u}}} + \mathbf{H}\bar{\mathbf{u}} - \mathbf{G}\bar{\mathbf{p}} + \mathbf{C}\bar{\mathbf{c}} = \mathbf{f} \tag{43a}$$

$$\mathbf{G}^{\mathrm{T}}\bar{\mathbf{u}} + \hat{\mathbf{L}}\bar{\mathbf{p}} + \mathbf{Q}\bar{\boldsymbol{\pi}} = \mathbf{0} \tag{43b}$$

$$\hat{\mathbf{C}}\bar{\mathbf{u}} + \mathbf{M}\bar{\mathbf{c}} = \mathbf{0} \tag{43c}$$

$$\mathbf{Q}^{\mathrm{T}}\bar{\mathbf{p}} + \hat{\mathbf{M}}\bar{\boldsymbol{\pi}} = \mathbf{0} \tag{43d}$$

where

$$\mathbf{H} = \mathbf{A} + \mathbf{K} + \hat{\mathbf{K}}$$

The matrices and vectors in the above equations are assembled from the element contributions in the standard manner. The element expressions for 3D problems are given next

$$\mathbf{M}^{\mathrm{e}}_{ij} = \int_{\Omega^{\mathrm{e}}} \rho N^i N^j \mathbf{I}_3 \,\mathrm{d}\Omega, \quad \mathbf{C}^{\mathrm{e}}_{ij} = \frac{1}{2}\int_{\Omega^{\mathrm{e}}} \begin{bmatrix} \mathbf{h}_1^{\mathrm{T}}\nabla N^i & 0 & 0 \\ 0 & \mathbf{h}_2^{\mathrm{T}}\nabla N^i & 0 \\ 0 & 0 & \mathbf{h}_3^{\mathrm{T}}\nabla N^i \end{bmatrix} N^j \,\mathrm{d}\Omega$$

$$\mathbf{A}^{\mathrm{e}}_{ij} = \int_{\Omega^{\mathrm{e}}} \rho N^i (\mathbf{u}^{\mathrm{T}}\nabla N^j)\mathbf{I}_3 \,\mathrm{d}\Omega, \quad \mathbf{K}^{\mathrm{e}}_{ij} = \int_{\Omega^{\mathrm{e}}} \mathbf{B}_i^{\mathrm{T}}\mathbf{D}\mathbf{B}_j \,\mathrm{d}\Omega, \quad \hat{\mathbf{K}}^{\mathrm{e}}_{ij} = \int_{\Omega^{\mathrm{e}}} (\bar{\nabla} N^i)^{\mathrm{T}}\bar{\mathbf{D}}\bar{\nabla} N^j \,\mathrm{d}\Omega$$

$$\mathbf{G}^{\mathrm{e}}_{ij} = \int_{\Omega^{\mathrm{e}}} \mathbf{B}_i^{\mathrm{T}}\mathbf{m} N^j \,\mathrm{d}\Omega, \quad \hat{L}^{\mathrm{e}}_{ij} = \int_{\Omega^{\mathrm{e}}} (\nabla N^i)^{\mathrm{T}}[\boldsymbol{\tau}]\nabla N^j \,\mathrm{d}\Omega$$

$$\mathbf{Q}^{\mathrm{e}}_{ij} = \int_{\Omega^{\mathrm{e}}} (\nabla N^i)^{\mathrm{T}} N^j [\boldsymbol{\tau}] \,\mathrm{d}\Omega, \quad \hat{\mathbf{C}}_{ij} = \int_{\Omega^{\mathrm{e}}} \rho^2 N^i (\mathbf{u}^{\mathrm{T}}\nabla N^j)\mathbf{I}_3 \,\mathrm{d}\Omega$$

$$\hat{\mathbf{M}}_{ij} = \int_{\Omega^{\mathrm{e}}} N^i N^j [\boldsymbol{\tau}] \,\mathrm{d}\Omega, \quad \mathbf{m} = [1, 1, 1, 0, 0, 0]^{\mathrm{T}}, \quad \mathbf{h}_i = [h_{i1}, h_{i2}, h_{i3}]^{\mathrm{T}}$$

$$\bar{\mathbf{D}} = \frac{\rho}{2}\begin{bmatrix} \mathbf{h}_1\mathbf{u}^{\mathrm{T}} & \mathbf{0} & \mathbf{0} \\ \mathbf{0} & \mathbf{h}_2\mathbf{u}^{\mathrm{T}} & \mathbf{0} \\ \mathbf{0} & \mathbf{0} & \mathbf{h}_3\mathbf{u}^{\mathrm{T}} \end{bmatrix}, \quad \bar{\nabla} = \begin{bmatrix} \nabla & \mathbf{0} & \mathbf{0} \\ \mathbf{0} & \nabla & \mathbf{0} \\ \mathbf{0} & \mathbf{0} & \nabla \end{bmatrix}$$

$$\nabla = \begin{Bmatrix} \dfrac{\partial}{\partial x_1} \\ \dfrac{\partial}{\partial x_2} \\ \dfrac{\partial}{\partial x_3} \end{Bmatrix}, \quad [\boldsymbol{\tau}] = \begin{bmatrix} \tau_1 & 0 & 0 \\ 0 & \tau_2 & 0 \\ 0 & 0 & \tau_3 \end{bmatrix} \tag{44}$$

DOI: 10.1002/fld

$$\mathbf{B}_i = \begin{bmatrix} \dfrac{\partial N^i}{\partial x_1} & 0 & 0 \\ 0 & \dfrac{\partial N^i}{\partial x_2} & 0 \\ 0 & 0 & \dfrac{\partial N^i}{\partial x_3} \\ \dfrac{\partial N^i}{\partial x_2} & \dfrac{\partial N^i}{\partial x_1} & 0 \\ \dfrac{\partial N^i}{\partial x_3} & 0 & \dfrac{\partial N^i}{\partial x_1} \\ 0 & \dfrac{\partial N^i}{\partial x_3} & \dfrac{\partial N^i}{\partial x_2} \end{bmatrix}, \quad \mathbf{D} = \mu \left(\begin{bmatrix} 2\mathbf{I}_3 & \mathbf{0} \\ \mathbf{0} & \mathbf{I}_3 \end{bmatrix} - \frac{2}{3}\mathbf{m}\mathbf{m}^{\mathrm{T}} \right)$$

$$\mathbf{I}_3 = \begin{bmatrix} 1 & 0 & 0 \\ 0 & 1 & 0 \\ 0 & 0 & 1 \end{bmatrix}, \quad \mathbf{f}_i = \int_{\Omega^{\mathrm{e}}} N^i \mathbf{b}\, \mathrm{d}\Omega + \int_{\Gamma^{\mathrm{e}}} N^i \mathbf{t}\, \mathrm{d}\Gamma$$

where $i, j, k = 1, n_{\mathrm{d}}$ in the above expressions.

A 3D finite element has typically 10 d.o.f.: three velocities $\bar{u}_i^k$, one pressure $\bar{p}^k$, three pressure gradient projections $\bar{\pi}_c^k$ and three convective projections $\bar{c}_i^k$, $i = 1, 2, 3$. Note, however, that the solution for the $\bar{\boldsymbol{\pi}}$ and $\bar{\mathbf{c}}$ variables is usually decoupled from the rest of equations and it is performed explicitly as shown in Section 8.

7. TRANSIENT SOLUTION SCHEME

The solution in time of the system of Equations (43) can be written in general form as

$$\mathbf{M}\frac{1}{\Delta t}(\bar{\mathbf{u}}^{n+1} - \bar{\mathbf{u}}^n) + \mathbf{H}^{n+\theta}\bar{\mathbf{u}}^{n+\theta} - \mathbf{G}\bar{\mathbf{p}}^{n+\theta} + \mathbf{C}^{n+\theta}\bar{\mathbf{c}}^{n+\theta} = \mathbf{f}^{n+\theta} \tag{45a}$$

$$\mathbf{G}^{\mathrm{T}}\bar{\mathbf{u}}^{n+\theta} + \hat{\mathbf{L}}^{n+\theta}\bar{\mathbf{p}}^{n+\theta} + \mathbf{Q}^{n+\theta}\bar{\boldsymbol{\pi}}^{n+\theta} = \mathbf{0} \tag{45b}$$

$$\hat{\mathbf{C}}^{n+\theta}\bar{\mathbf{u}}^{n+\theta} + \mathbf{M}\bar{\mathbf{c}}^{n+\theta} = \mathbf{0} \tag{45c}$$

$$[\mathbf{Q}^{n+\theta}]^{\mathrm{T}}\bar{\mathbf{p}}^{n+\theta} + \hat{\mathbf{M}}^{n+\theta}\bar{\boldsymbol{\pi}}^{n+\theta} = \mathbf{0} \tag{45d}$$

where $\mathbf{H}^{n+\theta} = \mathbf{H}(\bar{\mathbf{u}}^{n+\theta})$, etc. and the parameter $\theta \in [0, 1]$. The direct monolithic solution of Equations (45) is possible using an adequate iterative scheme. However, in our work we have used the fractional step method described next.

DOI: 10.1002/fld

8. FRACTIONAL STEP METHOD

A fractional step scheme is derived by splitting the discretized momentum equation (45a) into the following two equations:

$$\mathbf{M}\frac{1}{\Delta t}(\tilde{\mathbf{u}}^{n+1}-\bar{\mathbf{u}}^{n})+\mathbf{H}^{n+\theta}\tilde{\mathbf{u}}^{n+\theta}-\alpha\mathbf{G}\bar{\mathbf{p}}^{n}+\mathbf{C}^{n+\theta}\bar{\mathbf{c}}^{n+\theta}=\mathbf{f}^{n+\theta} \tag{46a}$$

$$\mathbf{M}\frac{1}{\Delta t}(\bar{\mathbf{u}}^{n+1}-\tilde{\mathbf{u}}^{n+1})-\mathbf{G}(\bar{\mathbf{p}}^{n+1}-\alpha\bar{\mathbf{p}}^{n})=\mathbf{0} \tag{46b}$$

In Equations (46) $\tilde{\mathbf{u}}^{n+1}$ is a predicted value of the velocity at time $n+1$ and α is a variable whose values of interest are zero and one. For $\alpha=0$ (first-order scheme) the splitting error is of order $0(\Delta t)$, whereas for $\alpha=1$ (second-order scheme) the error is of order $0(\Delta t^2)$ [19, 21]. We have chosen $\alpha=1$ for the solution of the examples presented in the paper.

Equations (46) are completed with the following three equations emanating from Equations (45b)–(45d)

$$\mathbf{G}^{\mathrm{T}}\bar{\mathbf{u}}^{n+1}+\hat{\mathbf{L}}^{n}\bar{\mathbf{p}}^{n+1}+\mathbf{Q}^{n}\bar{\boldsymbol{\pi}}^{n}=\mathbf{0} \tag{47a}$$

$$\hat{\mathbf{C}}^{n+1}\bar{\mathbf{u}}^{n+1}+\mathbf{M}\bar{\mathbf{c}}^{n+1}=\mathbf{0} \tag{47b}$$

$$[\mathbf{Q}^{n+1}]^{\mathrm{T}}\bar{\mathbf{p}}^{n+1}+\hat{\mathbf{M}}^{n+1}\bar{\boldsymbol{\pi}}^{n+1}=\mathbf{0} \tag{47c}$$

The value of $\bar{\mathbf{u}}^{n+1}$ obtained from Equation (47b) is substituted into Equation (47a) to give

$$\mathbf{G}^{\mathrm{T}}\tilde{\mathbf{u}}^{n+1}+\Delta t\mathbf{G}^{\mathrm{T}}\mathbf{M}^{-1}\mathbf{G}(\bar{\mathbf{p}}^{n+1}-\alpha\bar{\mathbf{p}}^{n})+\hat{\mathbf{L}}^{n}\mathbf{p}^{n+1}+\mathbf{Q}^{n}\bar{\boldsymbol{\pi}}^{n}=\mathbf{0} \tag{48}$$

The product $\mathbf{G}^{\mathrm{T}}\mathbf{M}^{-1}\mathbf{G}$ can be approximated by a Laplacian matrix, i.e.

$$\mathbf{G}^{\mathrm{T}}\mathbf{M}^{-1}\mathbf{G}=\frac{1}{\rho}\mathbf{L}\quad\text{with } L_{ij}=\int_{\Omega^{\mathrm{e}}}(\nabla N^{i})^{\mathrm{T}}\nabla N^{j}\,\mathrm{d}\Omega \tag{49}$$

The steps of the fractional step scheme (for $\alpha=1$) are as follows.

Step 1: Equation (46a) is linearized as

$$\mathbf{M}\frac{\tilde{\mathbf{u}}^{n+1}-\bar{\mathbf{u}}^{n}}{\Delta t}+\mathbf{H}^{n}\bar{\mathbf{u}}^{n}-\mathbf{G}\bar{\mathbf{p}}^{n}+\mathbf{C}^{n}\bar{\mathbf{c}}^{n}=\mathbf{f}^{n} \tag{50}$$

The fractional nodal velocities $\tilde{\mathbf{u}}^{n+1}$ can be explicitly computed from Equation (50) by

$$\tilde{\mathbf{u}}^{n+1}=\bar{\mathbf{u}}^{n}-\Delta t\mathbf{M}_{\mathrm{d}}^{-1}[\mathbf{H}^{n}\bar{\mathbf{u}}^{n}-\mathbf{G}\bar{\mathbf{p}}^{n}+\mathbf{C}^{n}\bar{\mathbf{c}}^{n}-\mathbf{f}^{n}] \tag{51}$$

Step 2: Compute $\bar{\mathbf{p}}^{n+1}$ from Equation (48) as

$$\bar{\mathbf{p}}^{n+1}=-\left[\hat{\mathbf{L}}^{n}+\frac{\Delta t}{\rho}\mathbf{L}\right]^{-1}\left[\mathbf{G}^{\mathrm{T}}\tilde{\mathbf{u}}^{n+1}-\frac{\Delta t}{\rho}\mathbf{L}\bar{\mathbf{p}}^{n}+\mathbf{Q}^{n}\bar{\boldsymbol{\pi}}^{n}\right] \tag{52}$$

Step 3: Compute $\bar{\mathbf{u}}^{n+1}$ explicitly from Equation (46b) as

$$\bar{\mathbf{u}}^{n+1}=\tilde{\mathbf{u}}^{n+1}+\Delta t\mathbf{M}_{\mathrm{d}}^{-1}\mathbf{G}(\bar{\mathbf{p}}^{n+1}-\bar{\mathbf{p}}^{n}) \tag{53}$$

DOI: 10.1002/fld

Step 4: Compute $\bar{\mathbf{c}}^{n+1}$ explicitly from Equation (47b) as

$$\bar{\mathbf{c}}^{n+1} = -\mathbf{M}_{\mathrm{d}}^{-1}\hat{\mathbf{C}}^{n+1}\bar{\mathbf{u}}^{n+1} \tag{54}$$

Step 5: Compute $\bar{\boldsymbol{\pi}}^{n+1}$ explicitly from Equation (47c) as

$$\bar{\boldsymbol{\pi}}^{n+1} = -\hat{\mathbf{M}}_{\mathrm{d}}^{-1}[\mathbf{Q}^{n+1}]^{\mathrm{T}}\bar{\mathbf{p}}^{n+1} \tag{55}$$

In the above equations $\mathbf{M}_{\mathrm{d}}$ and $\hat{\mathbf{M}}_{\mathrm{d}}$ denote the lumped diagonal form of matrices $\mathbf{M}$ and $\hat{\mathbf{M}}$, respectively.

Steps 1–5 are repeated until convergence for $\bar{\mathbf{u}}^{n+1}$, $\bar{\mathbf{p}}^{n+1}$, $\bar{\mathbf{c}}^{n+1}$ and $\bar{\boldsymbol{\pi}}^{n+1}$ is found. Typically, three iterations per time step sufficed to find a converged solution in the examples presented in the paper.

Above algorithm has improved stabilization properties *versus* the standard pressure segregation methods due to the introduction of the Laplacian matrix $\hat{\mathbf{L}}$ in Equation (52) which emanates from the FIC stabilization terms.

The boundary conditions are applied as follows. No condition is applied in the computation of the fractional velocities $\tilde{\mathbf{u}}^{n+1}$ in Equation (51). The prescribed velocities at the boundary are applied when solving for $\bar{\mathbf{u}}^{n+1}$ in the Step 3. The prescribed pressures at the boundary are imposed by making $\bar{\mathbf{p}}^{n}$ equal to the pressure values computed explicitly from the Neumann boundary condition (19a), neglecting the stabilization terms, i.e.

$$p^n = \frac{1}{3}\sum_i (s_{ij}^n n_j - t_i), \quad i = 1, n_{\mathrm{d}} \tag{56}$$

Equation (56) shows that for low values of the viscosity, the standard assumption of $p^n = 0$ on free surfaces (with $t_i = 0$) can be used.

We note that there is no need to prescribe any value of the pressure at the boundary if the form of matrix $\mathbf{L} = \rho\mathbf{G}^{\mathrm{T}}\mathbf{M}^{-1}\mathbf{G}$ as deduced from Equation (48) is used. This expression for $\mathbf{L}$ has a wider bandwidth than the Laplacian form of Equation (48) and therefore it is more inconvenient for practical purposes. In our work, we have used for $\mathbf{L}$ the simple Laplacian form of Equation (49).

9. COMPUTATION OF THE CHARACTERISTIC DISTANCES

The computation of the stabilization parameters is a crucial issue as they affect both the stability and accuracy of the numerical solution. The different procedures to compute the stabilization parameters are typically based on the study of simplified forms of the stabilized equations [1–28].

Recent work of the authors has shown that the stabilizing FIC terms for convection–diffusion problems take the form of a simple orthotropic diffusion if the balance equation is written in the principal curvature directions of the solution. Excellent results were reported in [45, 47] by computing first the characteristic length distances along the principal curvature directions, followed by a standard transformation of these distances to global axes. The resulting stabilized finite element equations capture the high gradient zones in the vicinity of the domain edges (boundary layers) as well as the sharp gradients appearing randomly in the interior of the domain [45, 47]. The FIC/FEM thus reproduces the best features of the so-called transverse (cross-wind) dissipation or shock-capturing methods [25, 26].

DOI: 10.1002/fld

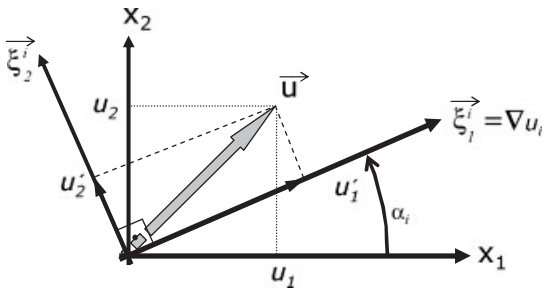

Figure 6. Definition of the principal curvature direction ξ_1^i along the gradient of u_i.

Let us assume that there exists at each point a local orthogonal coordinate system characterized by the local directions ξ_j^i with associated vectors $\boldsymbol{\xi}_j^i$ ($j=1,2$ for 2D problems) such that $\partial^2 u_i'/\partial\xi_j^i\partial\xi_k^i=0$ for $j\neq k$, where u_i' is the velocity component along the ξ_i^i direction (Figure 6). The ith FIC momentum equation (23) written in such a local coordinate system reads

$$\rho\left[\frac{\partial u_i'}{\partial t}+u'_j\frac{\partial u_i'}{\partial\xi_j^i}\right]+\frac{\partial p}{\partial\xi_j^i}-\frac{\partial}{\partial\xi_j^i}(\mu+\bar{\mu}_{jj})\frac{\partial u_i'}{\partial\xi_j^i}-b_i-\frac{h'_{ik}}{2}\frac{\partial c_i}{\partial\xi_k^i}+\mu\frac{\partial\varepsilon_v}{\partial\xi_i^i}=0 \tag{57}$$

The stabilizing dissipation introduced by the FIC approach has now the form of the orthotropic viscosity term underlined in Equation (57). For 2D problems

$$\frac{\partial}{\partial\xi_j^i}\bar{\mu}_{jj}\frac{\partial u_i'}{\partial\xi_j^i}=\frac{\partial}{\partial\xi_1^i}\left(\bar{\mu}_{11}\frac{\partial u_i'}{\partial\xi_1^i}\right)+\frac{\partial}{\partial\xi_2^i}\left(\bar{\mu}_{22}\frac{\partial u_i'}{\partial\xi_2^i}\right) \tag{58}$$

with

$$\bar{\mu}_{jj}=\frac{\rho u'_j h'_{ij}}{2}\quad\text{no sum in } j \tag{59}$$

The characteristic length distances h'_{ij} in Equation (57) are defined in the local axes $\boldsymbol{\xi}_j^i$. Note that the upper index i in vector $\boldsymbol{\xi}_j^i$ denotes the ith momentum equation corresponding to the u_i' velocity, while index j denotes the local directions, i.e. ξ_1^i, ξ_2^i are the two local coordinate directions corresponding to the ith momentum equation (Figure 6).

The value of h'_{ij} can be estimated by analogy of Equation (57) with the linear 1D advection–diffusion equation

$$\rho u'_j\frac{\partial\phi}{\partial\xi_j^i}-\frac{\partial}{\partial\xi_j^i}(\mu+\bar{\mu}_{jj})\frac{\partial\phi}{\partial\xi_j^i}=0\quad\text{no sum in } i \tag{60}$$

where ϕ is the transported variable.

DOI: 10.1002/fld

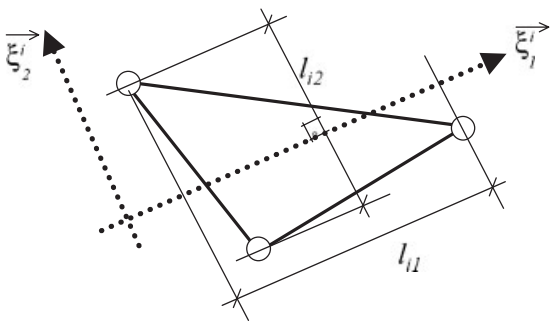

Figure 7. Definition of the element characteristic distances l_{i1} and l_{i2} corresponding to the ith momentum equation.

Introducing into Equation (60) the expression of $\bar{\mu}_{jj}$ of Equation (59) and assuming μ and $\bar{\mu}_{jj}$ to be independent of the space coordinates gives (for $\phi = u_i'$)

$$h'_{ij} = \left[2 \left(\frac{\partial u_i'}{\partial \xi_j^i} \right) \left(\frac{\partial^2 u_i'}{\partial \xi_j^{i2}} \right)^{-1} - \frac{1}{\gamma_{ij}} \right] l_{ij} = \alpha_{ij} l_{ij} \quad \text{no sum in } i, j \tag{61}$$

where

$$\alpha_{ij} = 2 \left(\frac{\partial u_i'}{\partial \xi_j^i} \right) \left(\frac{\partial^2 u_i'}{\partial \xi_j^{i2}} \right)^{-1} - \frac{1}{\gamma_{ij}}, \quad \gamma_{ij} = \frac{\rho u_i' l_{ij}}{2\mu} \tag{62}$$

and l_{ij} is a characteristic element dimension along the ξ_j^i direction (Figure 7).

Note that γ_{ij} can be interpreted as a local Reynolds number. It can be shown that $\alpha_{ij} \to 1$ for large values of γ_{ij} inducing high local gradients of the transported variable.

A good approximation for α_{ij} deduced by analogy with the stabilization parameter for the linear advection–diffusion equation [1, 37, 39] is

$$\alpha_{ij} = \coth \gamma_{ij} - \frac{1}{\gamma_{ij}} \tag{63}$$

Observation of Equation (63) shows that $\alpha_{ij} > 0.95$ for $\gamma_{ij} > 20$. Indeed, $\alpha_{ij} \simeq 1$ for high values of γ_{ij} typical of turbulent flows.

The characteristic distances h_{ij} are finally computed by transforming their local values h'_{ij} to global axes x_i. Details of the transformation are given below.

The numerical computations are simplified without apparent loss of accuracy if the ξ_1^i direction is taken to be constant within each element and equal to the direction of the gradient of the u_i velocity component at the element centre. The other coordinates ξ_j^i ($j = 2, 3$ for 3D problems) are defined so as to form an orthogonal system with ξ_1^i.

The algorithm described above for computing the characteristic distances h_{ij} is detailed below for 3D problems and linear tetrahedra elements. The particular form of some expressions for 2D problems using 3-noded linear triangles is given.

DOI: 10.1002/fld

For the ith momentum balance equation and every time step of the transient solution scheme:

1. A coordinate system ξ_1^i, ξ_2^i, ξ_3^i is defined at the element centre such that vector $\boldsymbol{\xi}_1^i$ is aligned with the gradient of u_i ($\boldsymbol{\xi}_1^i = \nabla u_i$), vector $\boldsymbol{\xi}_2^i$ is orthogonal to $\boldsymbol{\xi}_1^i$ in anticlockwise sense and vector $\boldsymbol{\xi}_3^i$ is defined by the vector product of $\boldsymbol{\xi}_1^i$ and $\boldsymbol{\xi}_2^i$. Figure 6 shows the definition of $\boldsymbol{\xi}_1^i$ and $\boldsymbol{\xi}_2^i$ for 2D problems.
2. The element characteristic distances l_{ij}, $j = 1, 2, 3$ are defined as the maximum projections of the element sides along the $\boldsymbol{\xi}_j^i$ axes (Figure 7).
3. The characteristic distances h_{ij}, $j = 1, 2, 3$ are computed as

$$\mathbf{h}_i = \mathbf{T}\mathbf{h}_i', \quad i = 1, 2 \tag{64}$$

with

$$\mathbf{T} = \begin{bmatrix} (1,1')^i & (1,2')^i & (1,3')^i \\ (2,1')^i & (2,2')^i & (2,3')^i \\ (3,1')^i & (3,2')^i & (3,3')^i \end{bmatrix}, \quad \mathbf{h}_i = \begin{Bmatrix} h_{i1} \\ h_{i2} \\ h_{i3} \end{Bmatrix}, \quad \mathbf{h}_i' = \begin{Bmatrix} h_{i1}' \\ h_{i2}' \\ h_{i3}' \end{Bmatrix} \tag{65}$$

where $(j,k)^i$ is the cosine of the angle between the global x_j-axis and the ξ_k^i-axis. For 2D problems

$$\mathbf{T} = \begin{bmatrix} c_i & -s_i \\ s_i & c_i \end{bmatrix} \tag{66}$$

where $c_i = \cos\alpha_i$, $s_i = \sin\alpha_i$ and α_i is the angle that ξ_1^i forms with the global axis x_1 (Figure 6). The local distances h_{ij}' are computed as

$$h_{ij}' = \left(\coth\gamma_{ij} - \frac{1}{\gamma_{ij}}\right) l_{ij}, \quad \gamma_{ij} = \frac{\rho u_j' l_{ij}}{2\mu}, \quad j = 1, 2 \tag{67}$$

where u_j' is the component of the velocity vector along the local axis $\boldsymbol{\xi}_j^i$ (Figure 6).

10. EXAMPLES

The first version of the FIC/FEM stabilized formulation presented above was successfully tested in a number of 2D problems including the flow over a backwards facing step and the flow past a cylinder. Excellent results were obtained for a range of Reynolds numbers as reported in [35]. The first 3D application of a flow past a cylinder at $Re = 1000$ also produced excellent results and it was briefly reported in [36]. The examples presented next provide further evidence of the effectiveness and accuracy of the FIC/FEM formulation presented in this paper for solving complex flows at high Reynolds numbers exhibiting turbulence effects.

DOI: 10.1002/fld

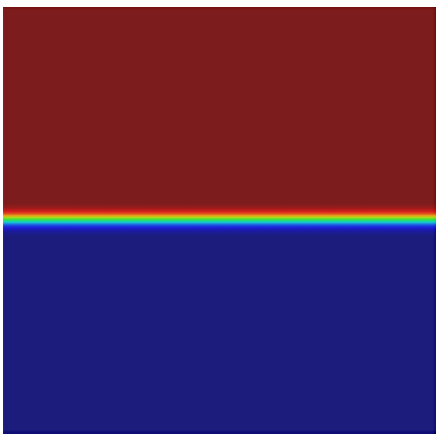

Figure 8. Initial configuration for the 2D mixing layer problem.

10.1. 2D mixing layer

We consider a temporal developing mixing layer [59], schematically sketched in Figure 8. The initial horizontal velocity has a hyperbolic-tangent profile:

$$u_1(x_2) = U \tanh\left(\frac{2x_2}{\delta_0}\right) \tag{68}$$

which implies a vorticity thickness

$$\delta_0 = \frac{2U}{\left.\dfrac{\mathrm{d}u_1}{\mathrm{d}x_2}\right|_{x_2=0}} \tag{69}$$

From linear stability analysis the mixing layer is known to be invisicidly unstable. A perturbation leads to the formation of vortices by Kelvin–Helmholtz instability, where the most amplified mode corresponds to a longitude wavelength $\delta = 7\delta_0$ [60]. Kelvin–Helmholtz instability leads to the development of vortices which in a later stage roll-up and merge.

The initial vorticity thickness δ_0 is chosen such that four vortices should develop in a square domain of unit size. In order to triggering the instability we superimposed a weak white noise in the rotational region. The value of $U = 1$ is chosen in Equation (68) and the viscosity is $\mu = 3.571 \times 10^{-6}$ (given a Reynolds number of 2.8×10^5). The boundary conditions applied are: periodic boundary conditions on the lateral boundaries and zero-normal-velocity and zero-shear-stress at the upper and bottom boundaries. With these boundary conditions, the problem is solved in a cylindrical domain.

We use a structured mesh of 256×256 3-noded triangular elements. Five hundred and seventy time steps of 0.0125 s lead to a total simulation time of 7.125 s.

The mixing layer is a good example for the tendency of 2D turbulence to transfer energy from small to large scales. This leads to a fast decrease of the complexity of the flow. In Figure 9 the vorticity modulus contours at several time steps is shown. Four vortices are formed as predicted by the linear theory, which subsequently undergo successive mergings.

DOI: 10.1002/fld

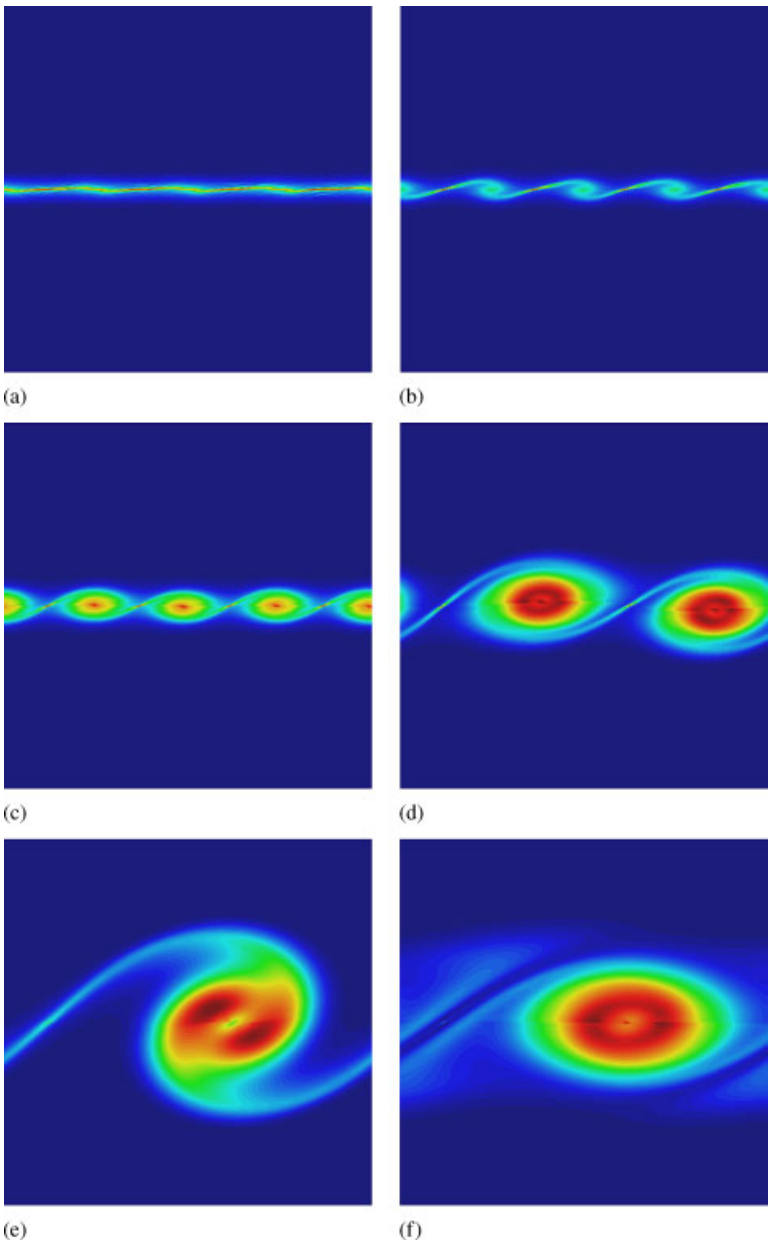

Figure 9. Vorticity modulus contours at times: (a) 0.5; (b) 0.75; (c) 1; (d) 2; (e) 3; and (f) 4 s.

For the reference simulations a Fourier spectral code was applied to the periodized version of the problem [61]. The code is based on the pressure–velocity formulation and uses a third order Adams–Bashforth (AB3) scheme. The numerical resolution was a grid of 256×256 too. Figure 10

DOI: 10.1002/fld

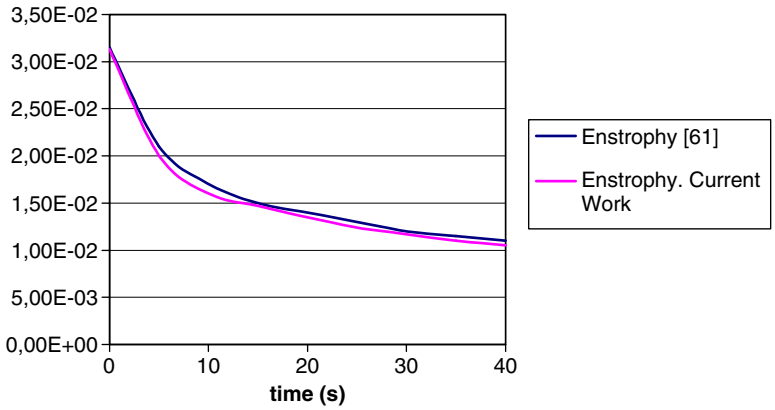

Figure 10. Enstrophy evolution with time.

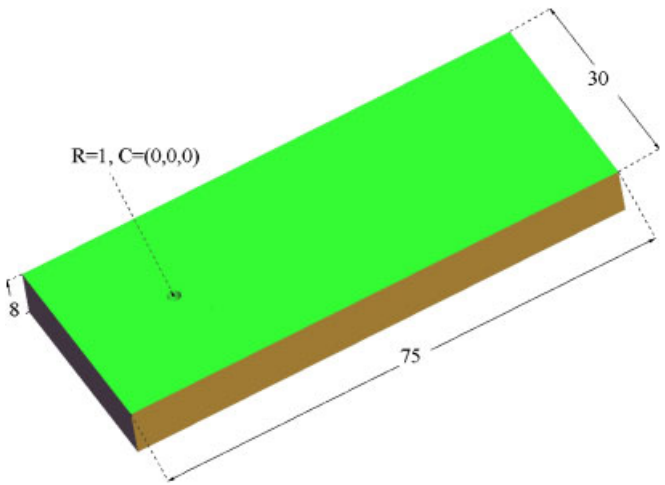

Figure 11. Computational domain for 3D flow past a cylinder.

compares the decay in time of the system enstrophy obtained with the reference run and with the present method. The results show that all the scales of the flow are well-resolved by the FIC formulation here proposed and compare well with the reference run.

10.2. 3D flow past a cylinder

We present a 3D simulation of unsteady incompressible flow around a circular cylinder. The simulation is performed at a Reynolds number of 10 000.

The diameter of the cylinder is 2 units and its length is 8 units (this length is recommended in [62] to capture a few wavelengths along the cylinder axis). The computation domain extends 15 units upstream, 60 units downstream, and 30 units in the cross-flow direction (Figure 11).

DOI: 10.1002/fld

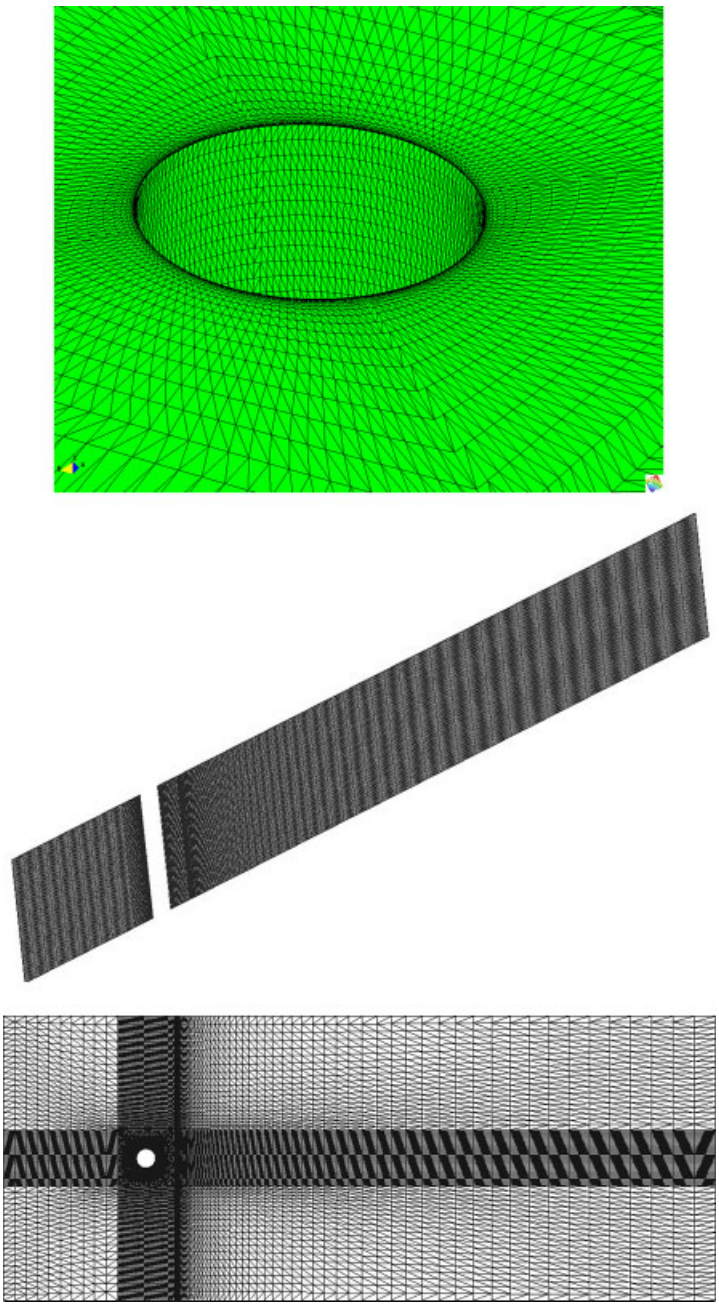

Figure 12. Flow past a cylinder. Details of the mesh used for the computations.

DOI: 10.1002/fld

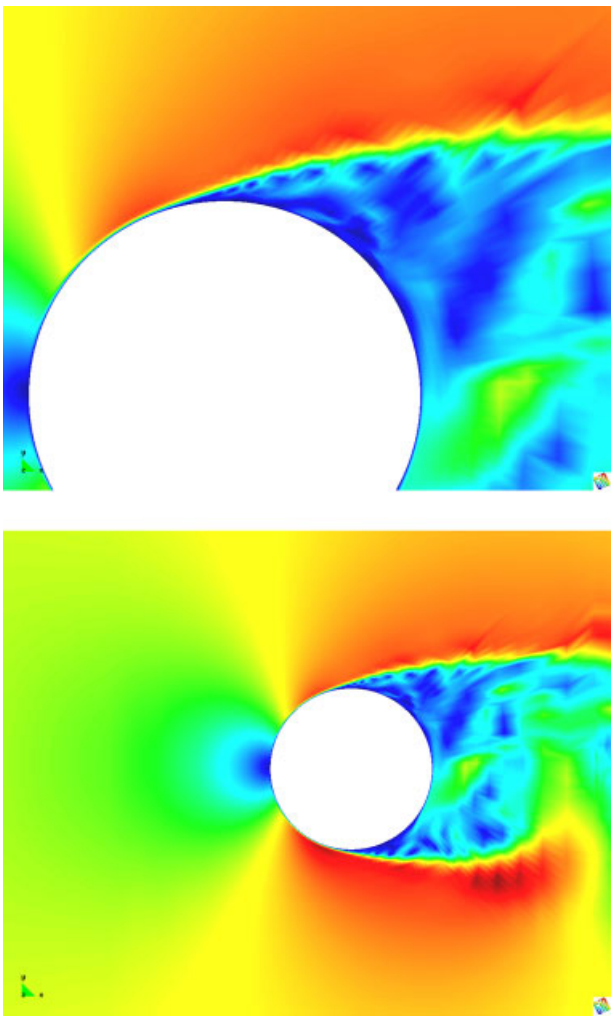

Figure 13. Velocity vector modulus contours in the plane $z = 4$ at time 50 s.

The boundary conditions consist of uniform inflow velocity set to 1.0, zero-normal-velocity and zero-shear-stress at the lateral boundaries, traction-free conditions at the outflow boundary and no-slip at the cylinder surface.

The computation presented here was carried out on a structured mesh of 5 193 600 linear tetrahedral elements (80 elements along the cylinder span and 160 along its circumference) and 864 270 nodes. The thickness of the layer of elements around the cylinder is 0.001. Figure 12 shows details of the mesh. For the simulation the time step is set to 0.025. The time-averaged drag coefficient is 1.07 and compares well with the value of 1.12 reported in experimental measurement [63, 64]. The Strouhal number is 2.02 and also agrees with experimental measurements [36, 38, 64].

DOI: 10.1002/fld

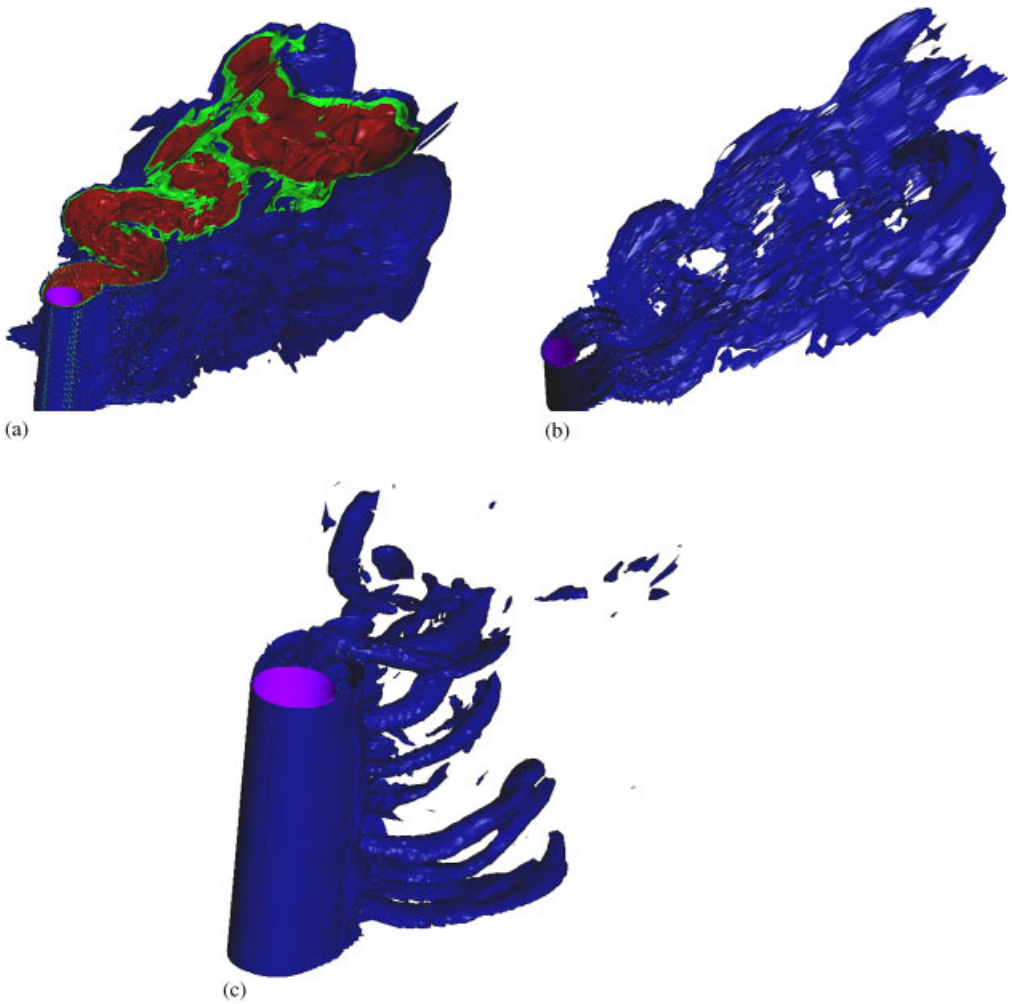

Figure 14. Vorticity vector modulus ω isosurfaces: (a) $\omega = 0.1, 0.2, 0.3$; (b) $\omega = 0.2$; and (c) $\omega = 2$.

The flow field in chordwise planes (perpendicular to the cylinder axis) reveals fine-scale structures. There is a clear difference between the turbulent wake and the laminar outer flow zones (see Figure 13). We observe the turbulent recirculating region bounded by shear layers. The shear layers roll up to produce small-scale vortices at the edge of the formation zone. These vortices cause entrainment of the free-stream fluid into the recirculating zone. The flow on the cylinder separates at an angle $\approx 78^\circ$ (measured from the leading stagnation point).

Figure 14 shows the isosurfaces of the vorticity vector modulus for three different vorticity values. Note that the flow structures are more diffuse due to the increasing turbulence effect.

Figure 15 shows streamlines behind the cylinder within the recirculation area. It is clear that the structure of the vortex is created in the turbulent region. When the vortex gets enough energy then it detaches from the cylinder, generating the von Karman street vortexes.

DOI: 10.1002/fld

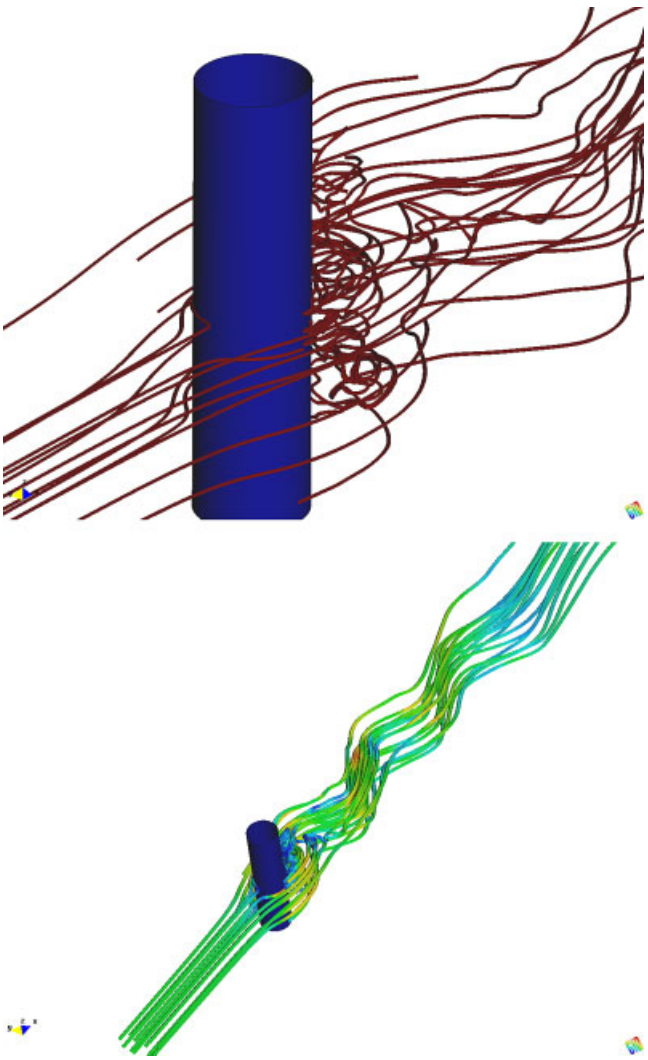

Figure 15. Streamlines at time $t = 50$.

11. CONCLUSIONS

The finite calculus (FIC) form of the Navier–Stokes equations is a good starting point for deriving stabilized FEM for solving a variety of incompressible fluid flow problems. The matrix stabilization terms introduced by the FIC formulation allow to obtaining physically sound solutions in the presence of sharp gradients occurring for high Reynolds numbers without the need of introducing a turbulence model. Good numerical solutions have been obtained in the 2D and 3D examples solved with relatively coarse meshes for high values of the Reynolds number inducing turbulence effects. These results reinforce our conviction that the stabilization terms introduced by the FIC formulation suffice to provide good results for problems for which turbulence models are required

DOI: 10.1002/fld

using alternative numerical methods. The results also confirm the close link between the stabilized methods and turbulence models.

ACKNOWLEDGEMENTS

The authors are grateful to Prof. S. R. Idelsohn for many useful suggestions. Thanks are also given to the company COMPASS Ingeniería y Sistemas SA (www.compassis.com) for providing the code Tdyn [65] where the presented formulation has been implemented.

This research was partially supported by project SEDUREC of the Consolider Programme of the Ministerio de Educación y Ciencia of Spain.

REFERENCES

1. Heinrich JC, Hayakorn PS, Zienkiewicz OC. An upwind finite element scheme for two dimensional convective transport equations. *International Journal for Numerical Methods in Engineering* 1977; **11**:131–143.
2. Kelly DW, Nakazawa S, Zienkiewicz OC. A note on anisotropic balancing dissipation in the finite element method approximation to convective diffusion problems. *International Journal for Numerical Methods in Engineering* 1980; **15**:1705–1711.
3. Brooks AN, Hughes TJR. Streamline upwind Petrov–Galerkin formulation for convective dominated flows with particular emphasis on the incompressible Navier–Stokes equations. *Computer Methods in Applied Mechanics and Engineering* 1982; **32**:199–259.
4. Donea J. A Taylor–Galerkin method for convective transport problems. *International Journal for Numerical Methods in Engineering* 1984; **20**:101–119.
5. Löhner R, Morgan K, Zienkiewicz OC. The solution of non-linear hyperbolic equation systems by the finite element method. *International Journal for Numerical Methods in Fluids* 1984; **4**:1043–1063.
6. Hughes TJR, Tezduyar TE. Finite element methods for first-order hyperbolic systems with particular emphasis on the compressible Euler equations. *Computer Methods in Applied Mechanics and Engineering* 1984; **45**:217–284.
7. Hughes TJR, Mallet M. A new finite element formulations for computational fluid dynamics. III. The generalized streamline operator for multidimensional advective–diffusive systems. *Computer Methods in Applied Mechanics and Engineering* 1986; **58**:305–328.
8. Hughes TJR, Franca LP, Balestra M. A new finite element formulation for computational fluid dynamics. V. Circumventing the Babuska–Brezzi condition: a stable Petrov–Galerkin formulation of the Stokes problem accommodating equal order interpolations. *Computer Methods in Applied Mechanics and Engineering* 1986; **59**: 85–99.
9. Hughes TJR, Franca LP, Hulbert GM. A new finite element formulation for computational fluid dynamics. VIII. The Galerkin/least-squares method for advective–diffusive equations. *Computer Methods in Applied Mechanics and Engineering* 1989; **73**:173–189.
10. Hirsch C. *Numerical Computation of Internal and External Flow*, vol. 1. Wiley: New York, 1990.
11. Franca LP, Frey SL. Stabilized finite element methods. II. The incompressible Navier–Stokes equations. *Computer Methods in Applied Mechanics and Engineering* 1992; **99**:209–233.
12. Tezduyar TE, Mittal S, Ray SE, Shih R. Incompressible flow computations with stabilized bilinear and linear equal order interpolation velocity–pressure elements. *Computer Methods in Applied Mechanics and Engineering* 1992; **95**:221–242.
13. Hughes TJR, Hauke G, Jansenn K. Stabilized finite element methods in fluids: inspirations, origins, status and recent developments. In *Recent Developments in Finite Element Analysis*, Taylor RL, Hughes TJR, Oñate E, Zienkiewicz OC (eds). International Center for Numerical Methods in Engineering (CIMNE): Barcelona, Spain, 1994; 272–292.
14. Hughes TJR. Multiscale phenomena: Green functions, subgrid scale models, bubbles and the origins of stabilized methods. *Computer Methods in Applied Mechanics and Engineering* 1995; **127**:387–401.
15. Storti M, Nigro N, Idelsohn SR. Steady state incompressible flows using explicit schemes with an optimal local preconditioning. *Computer Methods in Applied Mechanics and Engineering* 1995; **124**:231–252.
16. Cruchaga MA, Oñate E. A finite element formulation for incompressible flow problems using a generalized streamline operator. *Computer Methods in Applied Mechanics and Engineering* 1997; **143**:49–67.

DOI: 10.1002/fld

17. Codina R, Vazquez M, Zienkiewicz OC. A general algorithm for compressible and incompressible flow—Part III. The semi-implicit form. *International Journal for Numerical Methods in Fluids* 1998; **27**:13–32.
18. Cruchaga MA, Oñate E. A generalized streamline finite element approach for the analysis of incompressible flow problems including moving surfaces. *Computer Methods in Applied Mechanics and Engineering* 1999; **173**:241–255.
19. Codina R, Blasco J. Stabilized finite element method for the transient Navier–Stokes equations based on a pressure gradient operator. *Computer Methods in Applied Mechanics and Engineering* 2000; **182**:277–301.
20. Tezduyar TE, Osawa Y. Finite element stabilization parameters computed from element matrices and vectors. *Computer Methods in Applied Mechanics and Engineering* 2000; **190**:411–430.
21. Codina R, Zienkiewicz OC. CBS versus GLS stabilization of the incompressible Navier–Stokes equations and the role of the time step as stabilization parameter. *Communications in Numerical Methods in Engineering* 2002; **18**(2):99–112.
22. Codina R. Stabilized finite element approximation of transient incompressible flows using orthogonal subscales. *Computer Methods in Applied Mechanics and Engineering* 2002; **191**:4295–4321.
23. Nithiarasu P. An efficient artificial compressibility (AC) scheme based on the characteristic based split (CBS) method for incompressible flows. *International Journal for Numerical Methods in Engineering* 2003; **56**: 1815–1845.
24. Tezduyar TE. Computation of moving boundaries and interfaces and stabilization parameters. *International Journal for Numerical Methods in Fluids* 2003; **43**:555–575.
25. Donea J, Huerta A. *Finite Element Method for Flow Problems*. Wiley: New York, 2003.
26. Zienkiewicz OC, Taylor RL, Nietharasu P. *The Finite Element Method*, vol. 3. Elsevier: Amsterdam, 2005.
27. Tezduyar TE, Sathe S. Enhanced-approximation linear solution technique (EALST). *Computer Methods in Applied Mechanics and Engineering* 2004; **193**:2033–2049.
28. Tezduyar TE, Sathe S. Enhanced-discretization successive update method (EDSUM). *International Journal for Numerical Methods in Fluids* 2005; **47**:633–654.
29. Dubois T, Jauberteau F, Temam R. Incremental unknowns, multilevel methods and the numerical simulation of turbulence. *Computer Methods in Applied Mechanics and Engineering* 1998; **159**:123–189.
30. Dubois T, Jauberteau F, Temam R. *Dynamic Multilevel Methods and the Numerical Simulation of Turbulence*. Cambridge University Press: Cambridge, 1999.
31. Hughes TJR, Mazzei L, Jansen KE. Large eddy simulation and the variational multiscale method. *Computing and Visualization in Science* 2000; **3**:47–59.
32. Hughes TJR, Mazzei L, Oberai AA, Wray AA. The multiscale formulation of large eddy simulation: decay of homogeneous isotropic turbulence. *Physics of Fluids* 2001; **13**:505–512.
33. Hughes TJR, Oberai AA, Mazzei L. Large eddy simulation of turbulent channel flows by the variational multiscale method. *Physics of Fluids* 2001; **13**(6):1784–1799.
34. Hoffman J, Johnson C. A new approach to computational turbulence modeling. *Computer Methods in Applied Mechanics and Engineering* 2006; **195**:2865–2880.
35. Oñate E, Valls A, García J. FIC/FEM formulation with matrix stabilizing terms for incompressible flows at low and high Reynolds numbers. *Computational Mechanics* 2006; **38**(4–5):440–455.
36. Oñate E, Valls A, García J. Modeling incompressible flows at low and high Reynolds numbers via a finite calculus finite element approach. *Journal of Computational Physics* 2006, submitted.
37. Oñate E. Derivation of stabilized equations for advective–diffusive transport and fluid flow problems. *Computer Methods in Applied Mechanics and Engineering* 1998; **151**:233–267.
38. Oñate E. A stabilized finite element method for incompressible viscous flows using a finite increment calculus formulation. *Computer Methods in Applied Mechanics and Engineering* 2000; **182**(1–2):355–370.
39. Oñate E. Possibilities of finite calculus in computational mechanics. *International Journal for Numerical Methods in Engineering* 2004; **60**(1):255–281.
40. Oñate E, García J, Idelsohn SR. Computation of the stabilization parameter for the finite element solution of advective–diffusive problems. *International Journal for Numerical Methods in Fluids* 1997; **25**:1385–1407.
41. Oñate E, García J, Idelsohn SR. An alpha-adaptive approach for stabilized finite element solution of advective–diffusive problems with sharp gradients. In *New Advances in Adaptive Computational Methods in Mechanics*, Ladeveze P, Oden JT (eds). Elsevier: Amsterdam, 1998.
42. Oñate E, Manzan M. A general procedure for deriving stabilized space–time finite element methods for advective–diffusive problems. *International Journal for Numerical Methods in Fluids* 1999; **31**:203–221.

DOI: 10.1002/fld

43. Oñate E, Manzan M. Stabilization techniques for finite element analysis of convection–diffusion problems. In *Convection Heat Transfer*, Sunden B, Comini G (eds). WIT Press: Southampton, U.K., 2000; *Research Report PI183*, CIMNE, Barcelona, 2000.
44. Oñate E. Multiscale computational analysis in mechanics using finite calculus: an introduction. *Computer Methods in Applied Mechanics and Engineering* 2003; **192**(28–30):3043–3059.
45. Oñate E, Zárate F, Idelsohn SR. Finite element formulation for convective–diffusive problems with sharp gradients using finite calculus. *Computer Methods in Applied Mechanics and Engineering* 2006; **195**:1793–1825.
46. Oñate E, Miquel J, Hauke G. Stabilized formulation for the advection–diffusion–absorption equation using finite calculus and linear finite elements. *Computer Methods in Applied Mechanics and Engineering* 2006; **195**(33–36):3926–3946.
47. Oñate E, Miquel J, Zárate F. Stabilized solution of the multidimensional advection–diffusion–absorption equation using linear finite elements. *Computers and Fluids* 2007; **36**(1):92–112.
48. Felippa CA, Oñate E. Nodally exact Ritz discretizations of 1D diffusion–absorption and Helmholtz equations by variational FIC and modified equation methods. *Computational Mechanics* 2007; **39**(2):91–111.
49. Oñate E, García J. A finite element method for fluid–structure interaction with surface waves using a finite calculus formulation. *Computer Methods in Applied Mechanics and Engineering* 2001; **191**:635–660.
50. Idelsohn SR, Oñate E, Del Pin F. A lagrangian meshless finite element method applied to fluid–structure interaction problems. *Computers and Structures* 2003; **81**:655–671.
51. Oñate E, Idelsohn SR, Del Pin F, Aubry R. The particle finite element method. An overview. *International Journal of Computational Methods* 2004; **1**(2):267–307.
52. Idelsohn SR, Oñate E, Del Pin F. The particle finite element method: a powerful tool to solve incompressible flows with free-surfaces and breaking waves. *International Journal for Numerical Methods in Engineering* 2004; **61**:964–989.
53. Oñate E, García J, Idelsohn SR. Ship hydrodynamics. In *Encyclopedia of Computational Mechanics*, Stein E, de Borst R, Hughes TJR (eds), vol. 3, Chapter 18. Wiley: New York, 2004; 579–607.
54. Oñate E, García J, Idelsohn SR, Del Pin F. FIC formulations for finite element analysis of incompressible flows. Eulerian, ALE and Lagrangian approaches. *Computer Methods in Applied Mechanics and Engineering* 2006; **195**(23–24):3001–3037.
55. Oñate E, Rojek J, Taylor RL, Zienkiewicz OC. Finite calculus formulation for incompressible solids using linear triangles and tetrahedra. *International Journal for Numerical Methods in Engineering* 2004; **59**:1473–1500.
56. Oñate E, Taylor RL, Zienkiewicz OC, Rojek J. Aresidual correction method based on finite calculus. *Engineering Computations* 2003; **20**(5/6):629–658.
57. Rojek J, Oñate E, Taylor RL. CBS-based stabilization in explicit solid dynamics. *International Journal for Numerical Methods in Engineering* 2006; **66**:1547–1568.
58. Limache A, Idelsohn SR, Rossi R, Oñate E. The violation of objectivity in Laplace formulations of the Navier–Stokes equations. *International Journal for Numerical Methods of Fluids* 2007, submitted.
59. Lesieur M, Staquet C, Le Roy P, Comte P. The mixing layer and its coherence examined from the point of view of two dimensional turbulence. *Journal of Fluid Mechanics* 1998; **192**:511–535.
60. Michalke A. On the inviscid instability of the hyperbolic tangent velocity profile. *Journal of Fluid Mechanics* 1964; **19**:543–556.
61. Griebel M, Koster F. Adaptive wavelet solvers for the unsteady incompressible Navier–Stokes equations. In *Advances in Mathematical Fluid Mechanics*, Malek J, Rokyta M (eds). Springer: Berlin, 2000.
62. Kalro V, Tezduyar TE. Parallel 3D computation of unsteady flows around circular cylinders. *Parallel Computing* 1997; **23**:1235–1248.
63. Schlichting H. *Boundary-Layer Theory* (7th edn). McGraw-Hill: New York, 1979.
64. Gerard JH. An experimental investigation of the oscillating lift and drag of a circular cylinder shedding turbulent vortices. *Journal of Fluid Mechanics* 1961; **11**:244–256.
65. Tdyn. *A Finite Element Code for Fluid-Dynamic Analysis*. COMPASS Ingeniería y Sistemas SA, 2007 (Available from: www.compassis.com).

DOI: 10.1002/fld